(Received 13 March 2024, Accepted 16 April 2024, Scheduled 5 May 2024)

Wireless Power Transfer System for Cardiac Pacemakers Based on Multi-Coil Series Magnetic Integration

Xiaoheng Yan, Jinshu Yao*, Weihua Chen, and Yuhang Song

Faculty of Electrical and Control Engineering, Liaoning Technical University, Huludao 125000, China

ABSTRACT: We proposed a wireless power transfer system for cardiac pacemakers utilizing a multi-coil series magnetic integrated inductor-capacitor-capacitor/none (LCC-N) circuit topology operating at 50 kHz to reduce the volume of wireless power transfer systems for implanted pacemakers. Firstly, we established a mathematical model of LCC-N compensation topology and analyzed the relationship between the mutual inductance of the compensation and receiving coil and the system's transmission efficiency. The conclusion that the anti-offset performance of the system can be improved by using the change of the mutual inductance value was obtained. Secondly, the optimal coil structure was obtained via parameterized scanning, and a wireless power transfer system model for LCC-N was established for finite element simulation. The comparison of magnetic field strength was made between integrated and traditional non-integrated structures under aligned and offset conditions. Finally, the finite element simulation software ANSYS was adopted to establish a human body model, analyze the electromagnetic interference of the system to the human body, and evaluate the system's safety. Experimental results validated that the transmission efficiency of the system can reach 68.37%, and the output power was 1.47 W under multicoil series magnetic integrated structure when the transmission distance was 8 mm. The transmission efficiency remained 57.87% even with a horizontal offset of 8 mm, which is 13% higher than the traditional non-integrated structure.

1. INTRODUCTION

A pacemaker is an implantable medical device that stimulates cardiac muscle contraction and maintains an appropriate heart rate. Currently, implanted pacemakers are mainly powered by lithium batteries. However, a second surgical replacement is a rigid demand as the battery capacity is limited, leading to additional surgical risks and economic burdens to patients [1, 2]. Wireless power transfer (WPT) systems power implantable medical devices (IMDs) from in vitro and show unique advantages in solving the powering problems of implanted pacemakers [3–5] and have become the research focus of global scholars. However, problems like implant volume [6, 7], power transmission efficiency [8, 9], and electromagnetic compatibility [10] hinder the clinical application of WPT technology.

A large power current or voltage will be directly applied to the compensation capacitor when low-order compensation topologies are adopted [11, 12]. Global scholars conducted have much research on the application of high-order and hybrid compensation topologies in WPT systems. The introduction of compensation inductance and resonant capacitors leads to an increase in system volume. Therefore, research has been conducted to optimize the system structure and reduce the system size. Zhang et al. proposed a novel magnetic integrated structure with a primary single pole coil and a Double D-type compensation coil that decouples the same and opposite side primary and compensation coils used for a dual LCC topology. A transmission efficiency of 93.5% was achieved with transmitting and receiving coils aligned. However, the secondary resonant capacitors occupy a relatively large volume, leading to the inapplicability in in vivo environment [13]. Gu et al. proposed a control algorithm that can maintain stable output power under the dual changes of mutual inductance and load, improving the real-time performance of WPT systems without the need for DC-DC converters and wireless communication, reducing the complexity and weight of the system [14]. Zhang et al. proposed a receiving side topology simplification method utilizing the strong coupling between the transmitting and receiving coils, therefore reducing the reactive power of the receiving side, and the power transfer efficiency was maintained. However, the transmission efficiency of the S-N topology decreases rapidly when the coupling coefficient is low [15]. Yuan et al. proposed a novel dual-coupled inductor-capacitor-capacitor/series (LCC-S) compensation circuit design with reverse series compensation coils, and this structure can provide high misalignment tolerance and achieve constant output with zero phase angle (ZPA) input [16]. Xiao et al. proposed a detailed study on the pacemaker WPT system's safety and determined the optimal working frequency band based on inductor/capacitor/capacitor/series (LCC-C) topology. However, the research did not consider the volume issue of the compensating inductors [17]. Mahmood et al. presented a wireless power transmission system based on spider web-coil (SWC-MRC), which successfully achieved a 5 V DC voltage output when charging biomedical implant (BMI) devices. However, human body safety was not evaluated in the research, and the receiving coil is not suitable for implantation in animal or human bodies [18].

* Corresponding author: Jinshu Yao (y9274568@qq.com).

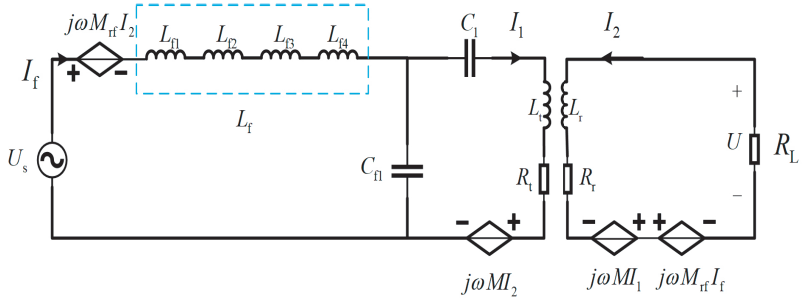

FIGURE 1. Equivalent circuit model of implantable pacemaker wireless power transfer system based on LCC-N compensation topology.

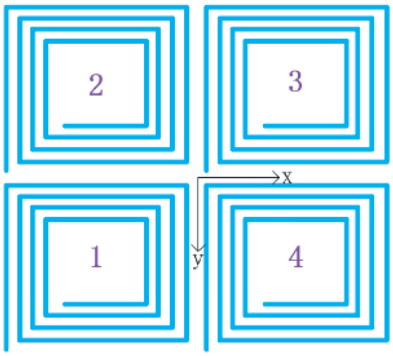

FIGURE 2. Schematic of primary side compensation coils.

To reduce the volume of the implanted part of WPT systems for cardiac pacemakers, we proposed an LCC-N cardiac pacemaker WPT system with multiple magnetically integrated series coils operating at 50 kHz [19]. The magnetic field strength distributions of integrated and traditional non-integrated structures were analyzed and compared by finite element simulation, and a human body model was established to analyze the electromagnetic interference of the system to human body. The system's safety was evaluated. An experimental system is constructed to validate the feasibility of the design. In short, the main contributions of this paper are given as follows.

1) The wireless power supply system of a multi-coil series magnetic integrated cardiac pacemaker using LCC-N proposed in this paper effectively reduces the number of devices required for implantation, making the system more compact and achieving the effect of reducing volume.

2) The resonant coil is used instead of the compensating inductor, and the compensating coil is integrated into four small coils in series to decouple the total equivalent inductance of the compensating coil from the transmitting coil. Furthermore, the mutual inductance between the compensation coil and receiving coil is utilized to improve the system's anti-offset performance.

2. SYSTEM CIRCUIT ANALYSIS BASED ON LCC-N COMPENSATION

2.1. LCC-N Compensation Circuit Model

The equivalent circuit model of WPT system for implantable cardiac pacemakers based on LCC-N compensation topology is shown in Figure 1. The specific in vivo working environment requires a minimized volume of the secondary side circuit. Compensation capacitors occupy a large volume and increase the weight and complexity of the implanted part. Therefore, this paper adopts LCC-N topology circuit with only the receiving coil in the implanted part to reduce the implanted volume. Besides, no additional compensation capacitors and inductors are needed. Such a circuit topology simplifies the structure of the secondary side circuit and reduces the implant's volume. Additionally, replacing the inductance in the compensation circuit with a resonant coil and integrating the coil into the transmitting coil aids in minimizing the overall volume of the system. The relationship among output power, transmission efficiency, and various parameters is analyzed based on the equivalent circuit model of the system. As shown in Figure 1, L_t and L_r are the inductances of the transmitting and receiving coils, respectively, with mutual inductance M between them. L_f is the inductance of the primary side compensation coil, which is divided into a series of four small coils denoted as L_{f1}, L_{f2}, L_{f3}, and L_{f4} with mutual inductance M_{rf} between them and the receiving coil. C_1 is the series compensation capacitor on the primary side. C_{f1} is the parallel compensation capacitor on the primary side. U_s is the inverter output voltage, and U is the voltage output to the load R_L. The resistance within the compensation network is disregarded in the equivalent circuit analysis as the resistance value is small.

A schematic of the series-connected primary side compensating coils is shown in Figure 2, where the four coils are labeled as 1, 2, 3, and 4, respectively. The outermost layer of each small coil represents the head, and the innermost layer represents the end. The connection method of the four small coils is as follows: the end of coil 1 is connected to the head of coil 2, the end of coil 2 connected to the end of coil 3, and finally the head of coil 3 connected to the end of coil 4. The directions of the current flow within each small coil are the same as the direction of the loop within each small coil. The mutual inductances between each small coil and the transmitting coil are M_{tf1}, M_{tf2}, M_{tf3}, and M_{tf4}, respectively, and are all equal in magnitude. The mutual inductances between each small coil and the receiving coil are denoted as M_{rf1}, M_{rf2}, M_{rf3}, and M_{rf4}, and are also equal in magnitude. $\dot{U}_{f1} \sim \dot{U}_{f4}$ represent the induced voltage on each small coil and are calculated as follows:

$$\begin{cases} \dot{U}_{f1} = j\omega M_{rf1}\dot{I}_2 + j\omega M_{tf1}\dot{I}_1 \\ \dot{U}_{f2} = j\omega M_{rf2}\dot{I}_2 + j\omega M_{tf2}\dot{I}_1 \\ \dot{U}_{f3} = -j\omega M_{rf3}\dot{I}_2 - j\omega M_{tf3}\dot{I}_1 \\ \dot{U}_{f4} = -j\omega M_{rf4}\dot{I}_2 - j\omega M_{tf4}\dot{I}_1 \end{cases} \tag{1}$$

The sum of the four induced voltages in (1) is 0. Therefore, although the coupling relationship exists between each small coil and the transmitting coil, the total equivalent inductance

is decoupled from the transmitting coil, ensuring the coupling coefficient between the compensating coil and the primary coil to be minimized. The impact of excess coupling on the system's transmission efficiency is reduced.

As the compensation coil and transmitting coil are decoupled, a total of two coupling coefficients exist among the transmitting coil, receiving coil, and compensation coil. k_{tr} is the coupling coefficient between the transmitting coil L_{t} and receiving coil L_{r}, and k_{rf} is the coupling coefficient between the receiving coil L_{r} and compensation coil L_f.

According to Kirchhoff's voltage law (KVL), the following equations can be obtained:

$$\begin{cases} j\omega L_{\mathrm{f}} I_1 + j\omega M_{\mathrm{rf}} I_2 = U_{\mathrm{s}} \\ j\omega M_{\mathrm{rf}} I_{\mathrm{f}} + j\omega M I_1 + (j\omega L_{\mathrm{r}} + R_{\mathrm{r}}) I_2 = U \\ j\omega L_{\mathrm{f}} I_{\mathrm{f}} + (1/j\omega C_{\mathrm{fl}} + 1/j\omega C_{\mathrm{l}} + j\omega L_{\mathrm{t}} + R_{\mathrm{t}} I_1 + j\omega M I_2 = 0 \end{cases} \tag{2}$$

where $Z = \frac{1}{j\omega C_{\mathrm{fl}}} + \frac{1}{j\omega C_{\mathrm{l}}} + j\omega L_{\mathrm{t}} + R_{\mathrm{t}}$ is the total impedance of the primary side.

In the LCC-N topology, the primary side is individually set as resonant. Therefore, the resonant angular frequency ω can be expressed as (3).

$$\omega = \frac{1}{\sqrt{L_{\mathrm{f}} C_{\mathrm{fl}}}} = \frac{1}{\sqrt{L_{\mathrm{t}} \frac{C_{\mathrm{fl}} C_{\mathrm{l}}}{C_{\mathrm{fl}} + C_{\mathrm{l}}}}} \tag{3}$$

The relationship between the current of the receiving coil I_2 and U_s can be solved by Equation (2) and is expressed by the following formula:

$$U_{\mathrm{s}} = I_2 \left[\left(j\omega L_{\mathrm{f}} \frac{j\omega L_{\mathrm{f}} R_{\mathrm{eq}} + \omega^2 M M_{\mathrm{rf}} - \omega^2 L_{\mathrm{r}} L_{\mathrm{f}} + j\omega L_{\mathrm{f}} R_{\mathrm{r}}}{j\omega M_{\mathrm{rf}} Z + \omega^2 M L_{\mathrm{f}}} \right) + j\omega M_{\mathrm{rf}} \right] \tag{4}$$

The equivalent load of the battery is R_{L}, and R_{eq} is the equivalent resistance of the system before the rectification circuit. The relationship between R_{eq} and R_{L} can be defined [20] as $R_{\mathrm{eq}} = \frac{8}{\pi^2} R_{\mathrm{L}}$.

The current flowing through the receiving coil I_2 can be simplified as:

$$I_2 = \frac{U_{\mathrm{s}} \left(j\omega M_{\mathrm{rf}} Z + \omega^2 M L_{\mathrm{f}} \right)}{A} \tag{5}$$

where $A = -R_{\mathrm{eq}}\omega^2 L_{\mathrm{f}}^2 + j2\omega^3 M M_{\mathrm{rf}} L_{\mathrm{f}} - j\omega^3 L_{\mathrm{r}} L_{\mathrm{f}} - \omega^2 M_{\mathrm{rf}}^2 Z - R_{\mathrm{r}}\omega^2 L_{\mathrm{f}}^2$.

The output power P_{out} of the system can be expressed as:

$$P_{\mathrm{out}} = |I_2|^2 R_{\mathrm{eq}} = 8 R_{\mathrm{L}} \left| \frac{U_{\mathrm{s}} \left(j\omega M_{\mathrm{rf}} Z + \omega^2 M L_{\mathrm{f}} \right)}{\pi A} \right|^2 \tag{6}$$

The current of the transmitting coil can be obtained from Equations (2) and (5) as follows:

$$I_1 = \frac{U_{\mathrm{s}} \left(j\omega R_{\mathrm{eq}} L_{\mathrm{f}} + \omega^2 M M_{\mathrm{rf}} - \omega^2 L_{\mathrm{f}} L_{\mathrm{r}} + j\omega L_{\mathrm{f}} R_{\mathrm{r}} \right)}{A} \tag{7}$$

The input current I_{f} is given by:

$$I_{\mathrm{f}} = \frac{U_{\mathrm{s}} \left(\omega L_{\mathrm{r}} Z - j R_{\mathrm{eq}} Z - j\omega^2 M^2 - j R_{\mathrm{r}} Z \right)}{jA} \tag{8}$$

The inverter output impedance Z_{in} is:

$$Z_{in} = \frac{jA}{(\omega L_{\mathrm{r}} Z - j R_{\mathrm{eq}} Z - j\omega^2 M^2 - j R_{\mathrm{r}} Z)} \tag{9}$$

The system input power P_{in} is:

$$P_{\mathrm{in}} = |I_f|^2 \,\mathrm{Real}\,(Z_{in}) \tag{10}$$

The system transmission efficiency is:

$$\eta_{\mathrm{trans}} = \frac{P_{\mathrm{out}}}{P_{\mathrm{in}}} \tag{11}$$

Equation (11) indicates that the system's transmission efficiency and output power are mainly affected by the load, the mutual inductance between the transmitting coil and receiving coil, and the mutual inductance between the compensation and receiving coils. With the magnitude of the load determined, the mutual inductance changes as horizontal offset of receiving coil occurs along the x or y axis. This change can be utilized to enhance the anti-offset performance of the system, thereby affecting the system's output power and transmission efficiency.

3. SYSTEM STRUCTURE AND SIMULATION ANALYSIS

3.1. Optimization of Primary Coil Structure

Power transfers between the primary and secondary sides of the WPT system via the primary coupling. Therefore, the objective of optimizing the coil structure is to obtain the optimal coupling coefficient between the transmitting and receiving coils. A comparison of coil shapes indicates that square spiral coils have better anti-misalignment performance than circular coils, making them more suitable for WPT systems [21]. Hence, the coil optimization of this work is based on tightly wound square spiral primary coils with zero spacing between turns. With the outer diameter of the coil and the distance between coil turns determined, the turn number of the coil becomes a critical parameter affecting the coupling coefficient, and the self-inductance of the coil also changes with the turn numbers. Therefore, studying the impact of these two parameters on the coupling coefficient is necessary for determining the optimal coil structure.

The structure optimization flowchart for the primary coil is shown in Figure 3. To simplify the study of coupling effects, the geometric shape and size of the transmitting and receiving coils were set to be consistent. According to the dimensions of the Medtronic G70 pacemaker (44.7 mm × 47.9 mm × 7.5 mm), the primary coil size was selected as 32 × 32 × 0.6 mm. The thickness and turn spacing of the primary coils were determined subsequently, and the transmission distance was set as 8 mm. The maximum coil turn number is 26 under zero turn spacing scenario. Finite element analysis was conducted based on the change of the coupling coefficient and self-inductance value

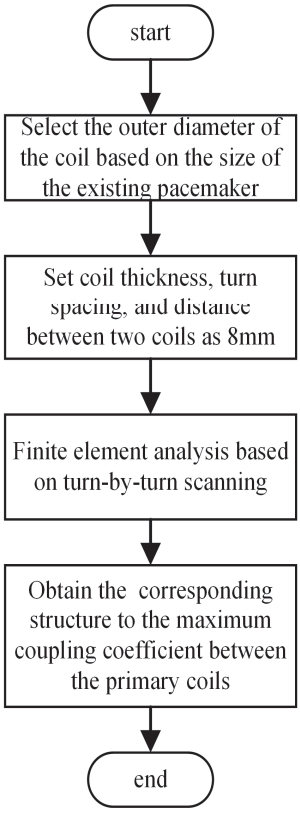

FIGURE 3. Primary coil structure optimization flowchart.

along with 0 to 26 turn number change of the coil. The optimal coil turn number is determined based on the optimal coupling coefficient of the primary coil, thereby obtaining the optimal coil structure. The optimization results are shown in Figure 4. When the coil turn spacing is 0, the coupling coefficient of the primary coil increases along with the turn number and reaches a maximum before decreasing. The coupling coefficient reaches its peak at 24 turns, indicating the optimal structure for the primary coil.

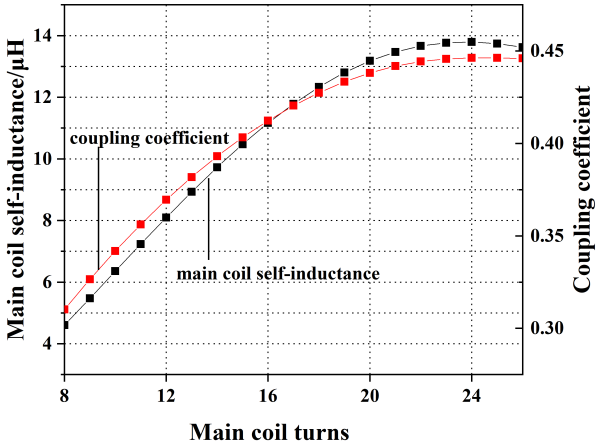

FIGURE 4. Coil optimization results.

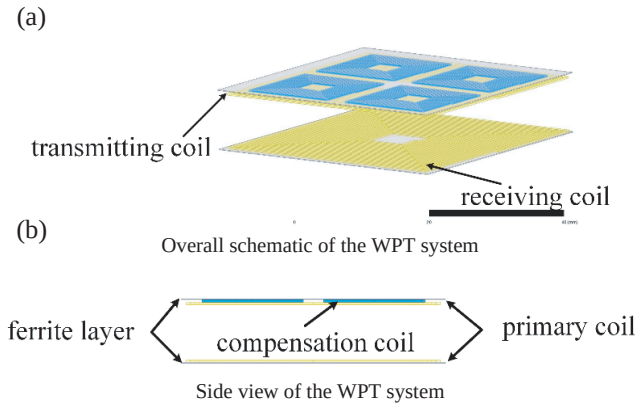

FIGURE 5. Coil structure. (a) Overall structure diagram. (b) Side view of the WPT system.

3.2. Coupling Mechanism Design

To validate the transmission characteristics of the integrated system, we selected the traditional non-integrated structure with independent inductors as compensation inductance as a comparative coupling mechanism. This paper adopted finite element simulation software ANSYS to model the system. The analysis was conducted under 50 kHz working frequency. According to the optimal structure acquired above, the final primary coil model was set as a 32 mm × 32 mm 24-turn square spiral structure. The series-connected compensation coils are modeled as 14 mm × 14 mm 16-turn square spiral structures based on calculations and simulation settings. Both primary and compensation coils are 0.3 mm thick. A 0.3 mm thin layer non-metallic ferrite magnetic material, measuring 35 mm × 35 mm, is applied externally to both the compensation and receiving coils. The ferrite film has a high relative permeability reaching several thousands to minimize the eddy current losses. The proposed integrated coil structure is shown in Figure 5, where L_t is the transmitting coil, and L_r is the receiving coil. The coil adopts a tight winding method, and the compensation coil is connected in series in the clockwise direction.

3.3. System Simulation Analysis

To analyze the impact of the integrated structure on power transfer and compare the integrated and traditional non-integrated system structures under same conditions, magnetic field intensity simulation in the xOz plane of both structures is conducted with varying transmission distances. The transmission distance ranges from 8 mm to 20 mm and changes with 6 mm step length. The system comparison simulation is shown in Figure 6.

The simulation results show that the thin ferrite film can effectively reduce the magnetic leakage between coils. As the transmission distance increases, the magnetic field strength of the system decreases in both structures. Comparison shows that the field intensity of integrated structure is superior to traditional structure at all transmission distances. Furthermore, as shown in the left diagrams of Figures 6(a), (b), and (c), the inte-

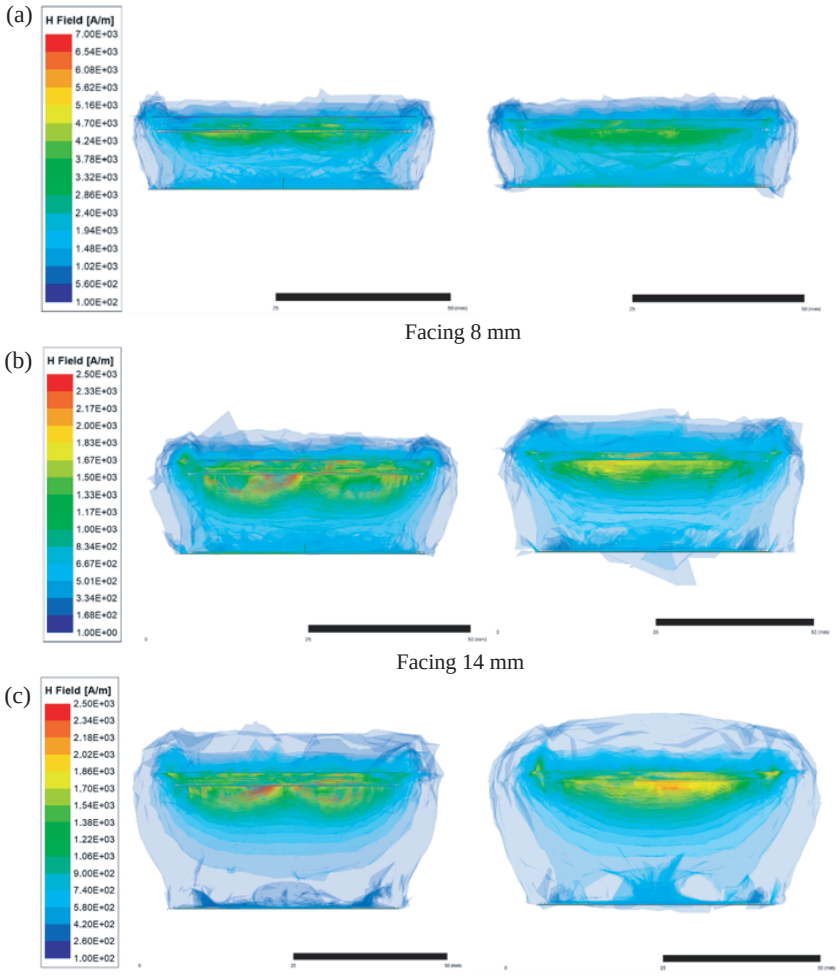

FIGURE 6. Magnetic field distribution comparison between integrated and traditional non-intergrated structures under different transmission distances (on the left side of each image is the integrated structure).

grated structure has a wider high magnetic field intensity region than traditional non-integrated structure.

WPT systems for cardiac pacemakers are more prone to horizontal misalignment. To analyze the positive impact of the mutual inductance introduced in the integrated structure on the system's transmission performance when misalignment occurs, we conducted horizontal misalignment simulations for both integrated and traditional structures. The maximum length of the coil is 32 mm, so the changes in magnetic field intensity of the receiving coil along the x-axis and y-axis offset by one-eighth and one-quarter of the coil's size were mainly compared, as shown in Figure 7 and Figure 8.

Simulation results show that in both offset situations, the magnetic field intensity decreases compared to the perfectly aligned situation. However, the coupling effect of the integrated structure is stronger than traditional structure under misaligned scenarios. Comparing Figure 7 and Figure 8, it can be observed that in integrated structure, the increase of magnetic field intensity near the receiving coil is more significant when the offset occurs on y-axis than x-axis. This phenomenon corresponds to the influence of the clockwise series connection of compensation coils on the magnetic field. The comparison of magnetic field intensity under two different structural offset situations also validates that the integrated structure can enhance the magnetic field intensity around the receiving coil as mutual inductance between the magnetic integrated compensation coil and receiving coil is introduced. The introduction of such mutual inductance also has a positive impact on the transmission performance of the system. Thereby, the transmission performance under system offset is further improved.

4. SAFETY ASSESSMENT

4.1. Evaluation Criteria

To prevent the electromagnetic field from harming the patients, WPT systems for implanted medical device require electromagnetic safety validation. When the receiving coil is placed in an alternating magnetic field, electromagnetic induction effect will happen, causing the temperature rise in the coils. The induced heat may cause tissue damage once it exceeds a certain threshold. To avoid such harm, the International Commis-

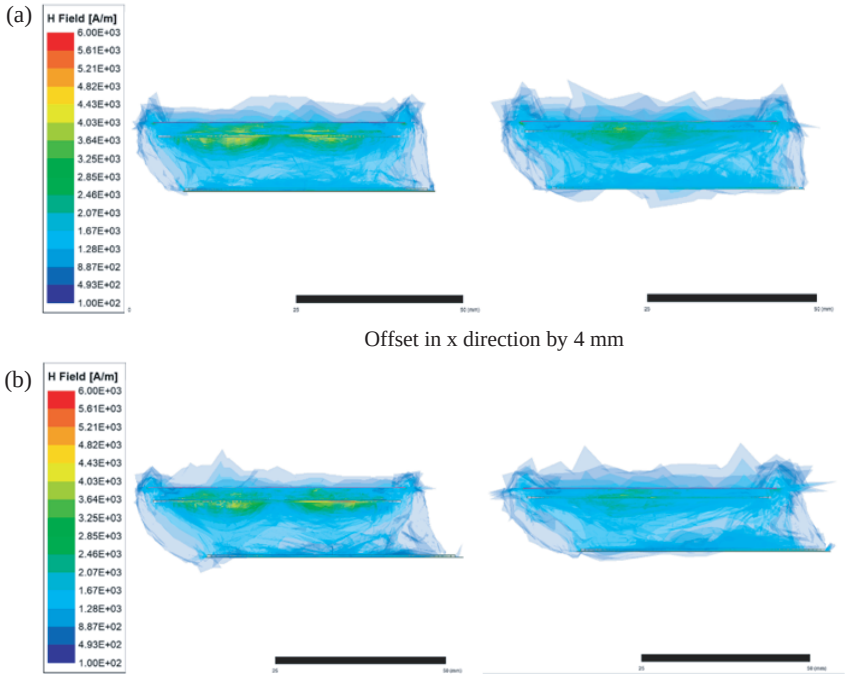

FIGURE 7. Magnetic field distribution diagram of the system with x-direction offset under two structures (on the left side of each image is the integrated structure).

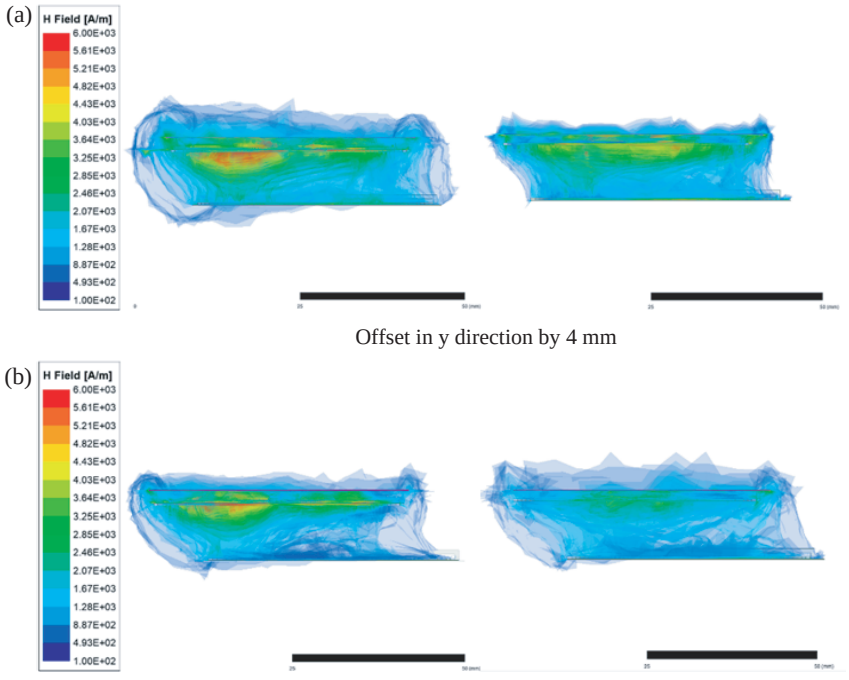

FIGURE 8. Magnetic field distribution of the system with y-direction offset under two structures (on the left side of each image is the integrated structure).

sion on Non-Ionizing Radiation Protection (ICNIRP) has established exposure limits for static and time-varying electromagnetic fields to provide high-level protection at different frequencies. According to the ICNIRP guidelines [22] and IEEE [23] standards, specific absorption rate (SAR) evaluation is not required for electromagnetic fields below 100 kHz. The peak limits for electric field strength and magnetic field intensity in human body are 13.5 V/m and 21 A/m at 50 kHz.

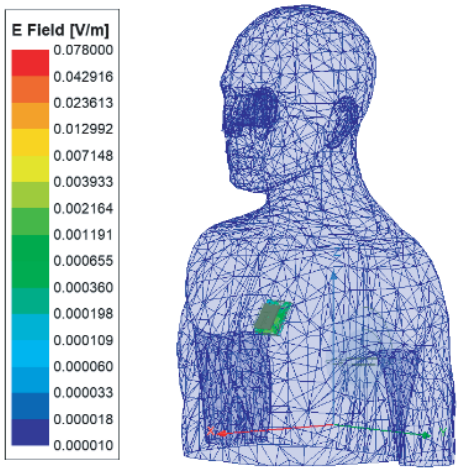

FIGURE 9. Distribution of electric field intensity in human body.

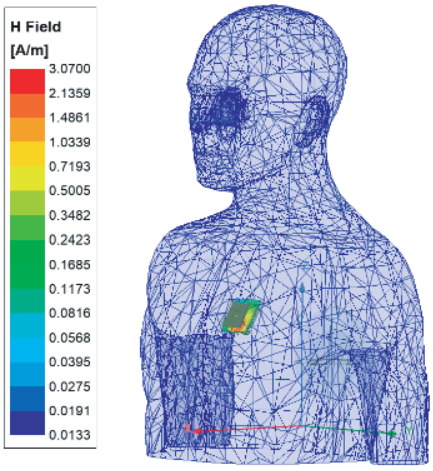

FIGURE 10. Distribution of magnetic field intensity in human body.

4.2. Human Body Model Construction

To evaluate the system's safety, we established a three-dimensional human body model in ANSYS. The model includes tissues such as the myocardium, fat, skin, and muscle. Electromagnetic parameters vary non-uniformly among different tissues, and the frequency has corresponding impacts on them. The electromagnetic parameters of various tissues differ at different frequencies. The relative permittivity and conductivity are the main parameters describing the electromagnetic properties of the human body. Table 1 shows the electromagnetic parameters of human tissues under 50 kHz. The tissue parameters are sourced from the official database of the IT'IS Foundation in Switzerland [24]. The values of tissue parameters adopted in the model are listed in Table 1.

TABLE 1. Electromagnetic parameters of human tissues at a working frequency of 50 kHz.

Human tissue	Relative permittivity	Electric Conductivity (S/m)
heart	17000	0.195
skin	1130	0.000273
fat	163	0.0433
muscle	10100	0.352

4.3. Electromagnetic Safety Assessment

As shown in Figure 9 and Figure 10, the transmitting coil is located outside the body, and the receiving coil is positioned beneath the chest tissue composed of 1 mm skin, 2 mm fat, and 5 mm muscle [25, 26]. Based on the aforementioned tissue characteristic, we conducted an electromagnetic safety analysis at 50 kHz. The electric field strength and magnetic field intensity within tissue are illustrated in Figure 9 and Figure 10.

Simulation results indicate that the maximum electric field strength is 0.078 V/m within chest tissue, which is significantly lower than the 13.5 V/m electric field limit standard. The safety standards are met, and the normal functionalities are not affected. The maximum magnetic field intensity is 3.07 A/m, which does not exceed the 21 A/m magnetic field intensity limit standard, thus complying with human safety regulations.

5. EXPERIMENTAL VERIFICATION

5.1. Experimental System Construction

To verify the power transfer and anti-misalignment performance of the proposed WPT system with multiple series-connected coils, we constructed a simulating experimental WPT system for implantable pacemakers, as shown in Figure 11. The experimental system consists of a DC power supply, an inverter circuit, a coupling mechanism, a rectifier, and a load. The transmission distance was set as 8 mm and the simulated human chest tissue composed of 1 mm pig skin, 2 mm fat, and 5 mm pork muscle. The experimental system, except for the DC power supply and oscilloscope, is placed in a transparent 25 cm $\times$ 30 cm $\times$ 60 cm box built with 2 mm-thick acrylic board to approximately simulate the in vivo working scenario with constant temperature.

The parameters of the experimental system are as shown in Table 2. The self-inductance of the primary coil is 13.3 µH; the series capacitance C_1 on the primary side is 3.78 µF; and the parallel capacitance on the primary side is 914 nF. The coils are integrated based on the simulation results. The integrated topology can effectively reduce the volume of the implantable devices and enhance the coupling. A thin layer of non-metallic ferrite magnetic material is added to the upper part of the compensation coil and receiving coil for magnetic and electrical shielding. The 50 kHz low frequency can effectively reduce the skin effect and proximity effect in the coil.

5.2. System Performance Experiment

The 5 V-1 A DC power provided by the power source is converted into 50 kHz AC power by the inverter circuit. The high-frequency AC power is transmitted from the transmitting coil to the receiving coil by the coupling structure and rectified to

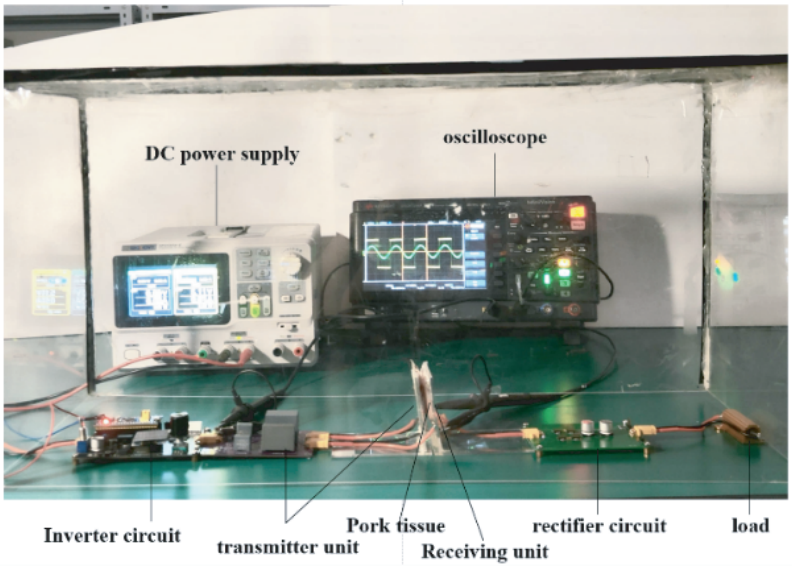

FIGURE 11. Experimental System.

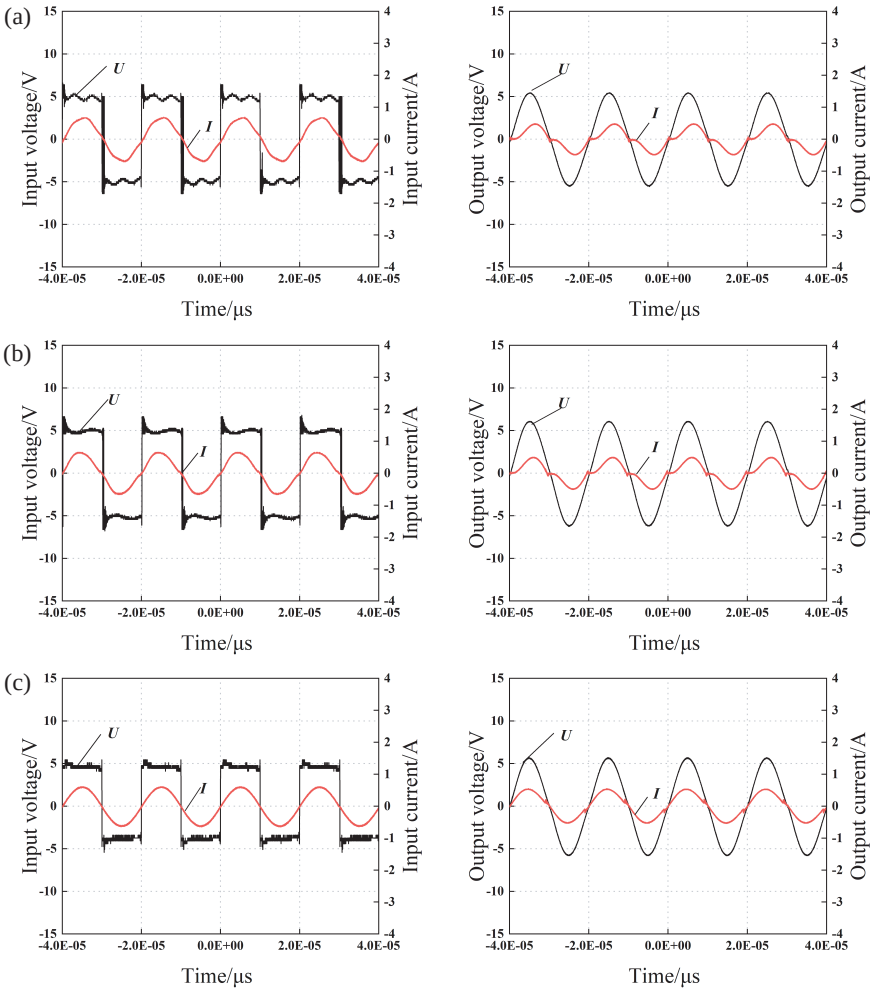

FIGURE 12. Comparison of input and output waveforms of the aligned system. (a) Input (output) voltage and current waveforms at 8 mm transmission distance in traditional non-integrated structure. (b) Input (output) voltage and current waveforms at 8 mm transmission distance in integrated structure. (c) Input (output) voltage and current waveforms at 8 mm transmission distance in the LCC-S structure of the system.

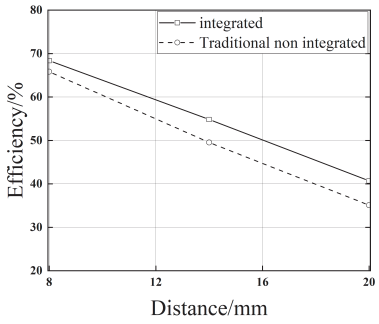

FIGURE 13. Comparison of transmission efficiency.

Element	Parameter
the transmitter (receiver) (μH)	13.3
individual compensation coils (μH)	2.1
C_{fl} (nF)	914
C_1 (μF)	3.78
size of the transmitter (receiver)	24 turns 32 mm × 32 mm
size of individual compensation coils	16 turns 14 mm × 14 mm
work frequency (kHz)	50

TABLE 2. WPT system parameters based on LCC-N.

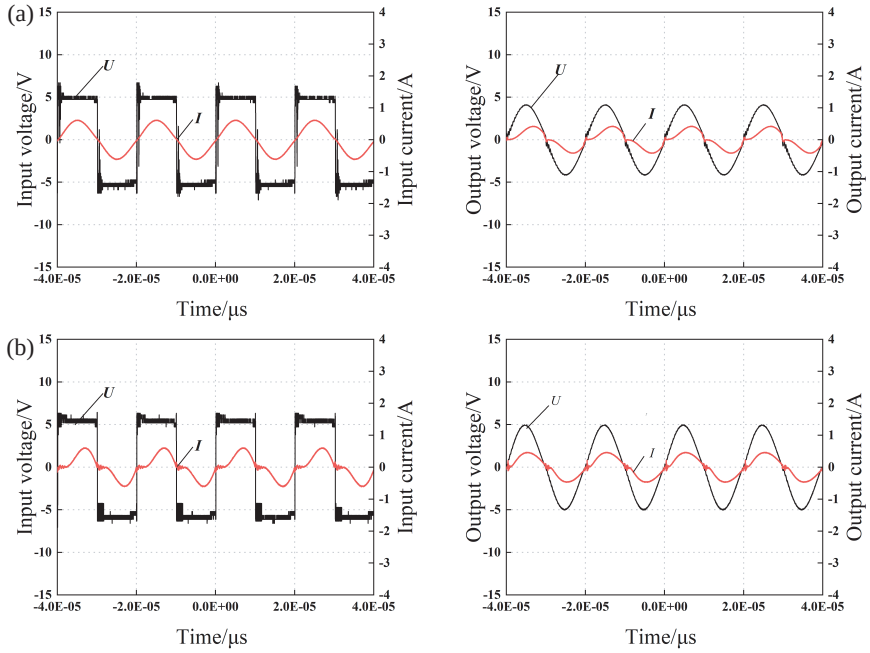

FIGURE 14. Comparison of input and output waveforms with an 8 mm offset in the x-axis of the system. (a) Input (output) voltage (current) waveform when the x-axis of the system is offset by 8 mm in traditional non-integrated structure. (b) Input (output) voltage (current) waveform when the x-axis of the system is offset by 8 mm in an integrated structure.

DC power output by the rectifying circuit. The pacemaker load is simulated by a power resistor.

To compare the transmission efficiency between integrated and traditional non-integrated system structures, we conducted experiments on two different system structures with transmission distance ranging from 8 to 20 mm. Three transmission distances of 8 mm, 14 mm, and 20 mm were selected for the comparative experiments. The peak value of voltage and current of the two structures at 8 mm transmission distance are shown in Figure 12(a) and Figure 12(b). The effective values of the electric parameters were adopted for transmission efficiency calculation. When the coils directly face each other at 8 mm distance, the transmission efficiency of the integrated structure system reaches 68.37%, with an output power of 1.47 W. Meanwhile, the transmission efficiency of the traditional non-integrated structure system is 65.83%. The integrated system showed a slight efficiency increase compared to the traditional non-integrated system with the volume of the implanted part significantly reduced, making it more suitable for implantable medical devices. The comparison of transmission efficiency at different transmission distances is shown in Figure 13.

To compare the transmission performance between the integrated system with reduced implantation volume and the traditional LCC-S system, we conducted comparative experiments for both structures at an 8 mm transmission distance along the z-axis. The experimental waveforms are shown in Figure 12(b) and Figure 12(c). Comparison results show that at the same transmission distance, the transmission efficiency of the traditional non-integrated LCC-S system was 71.66%, with little difference in transmission performance compared to the integrated structure. The presence of compensation capacitors in this system's secondary side circuit increases the implant's weight and

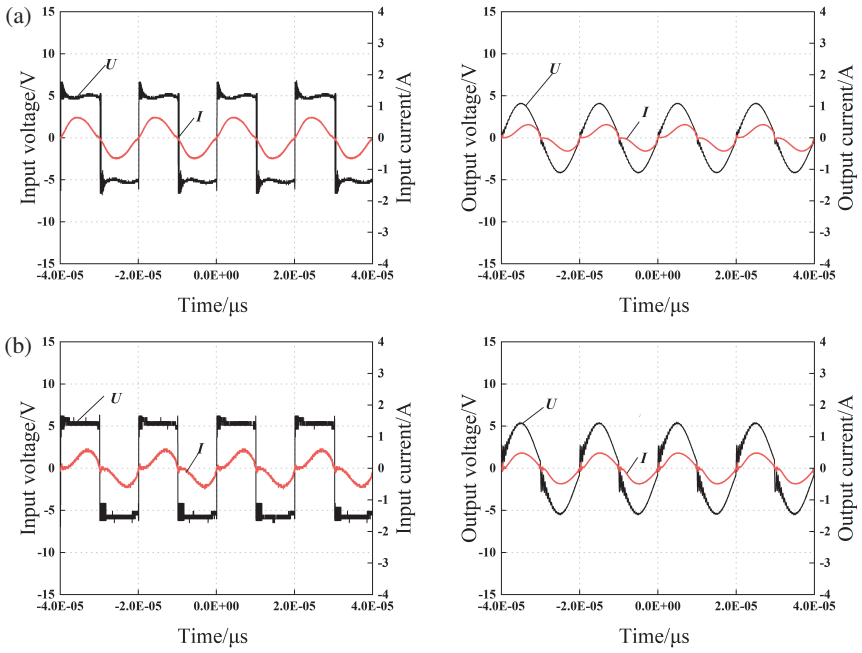

FIGURE 15. Comparison of input and output waveforms with a y-axis offset of 8 mm in the system. (a) Input (output) voltage (current) waveform when the y-axis of the system is offset by 8 mm in traditional non-integrated structure. (b) Input (output) voltage (current) waveform when the y-axis of the system is offset by 8 mm in an integrated structure.

volume. The experimental results indicated that the integrated structure reduces the volume of the secondary side with transmission performance not significantly affected.

To verify the anti-misalignment ability enhancement of the proposed integrated system, we conducted misaligned power transfer experiment at 8 mm transmission distance along the z-axis. With the central normal line of receiving coil kept parallel to the z-axis, two sets of anti-misalignment experiments were conducted at 4 mm and 8 mm transmission distances, respectively. The voltage and current waveforms comparison results are shown in Figure 14 and Figure 15. The transmission efficiency results are listed in Table 3. When the receiving coil was horizontally offset by 8 mm on x-axis and y-axis, respectively, the transmission efficiencies were 56.54% and 57.87% for the integrated structure. Compared to 43.22% and 44.09% for non-integrated structure, the efficiency results were approximately increased by 13.32% and 13.78%, respectively, indicating a positive impact on the anti-misalignment performance of the proposed integrated WPT system, further confirming the positive impacts of mutual inductance between the compensation coil and receiving coil on the system's transmission efficiency.

TABLE 3. Transmission efficiency comparison between two systems under horizontal offset.

Offset distance	Integrated structure	Traditional non-integrated structure
4 mm offset in the x-axis	60.28%	49.75%
4 mm offset in the y-axis	62.36%	53.69%
8 mm offset in the x-axis	56.54%	43.22%
8 mm offset in the y-axis	57.87%	44.09%

6. CONCLUSIONS

We proposed a WPT system operating at 50 kHz for cardiac pacemakers based on multi-coil series magnetic integration. The LCC-N compensation topology was adopted, and the primary compensation inductors were integrated in series with the transmitting coil. The system volume was reduced, and the structure of the WPT system became more compact with the transmission efficiency approximately not affected. The positive impact of mutual inductance between the compensation coil and receiving coil, including transmission efficiency preservation and anti-misalignment performance enhancement of the proposed integrated system were validated via finite element simulations and experiments. Transmission efficiencies of the proposed system at different misalignment scenarios significantly increased compared to the traditional non-integrated structure. Additionally, the electric and magnetic field intensities in human tissue are analyzed in a simulated human body model to validate the safety of the system to human body. The contributions and conclusions of this work are as follows:

1) The LCC-N compensation topology was adopted in the proposed design, and relationships among output power, transmission efficiency, and factors such as load, mutual inductance between the primary and compensation coils, and mutual inductance between the compensation and receiving coils were analyzed. The coupling relationship between the series connection structure of the primary side compensation coils and transmitting coil was analyzed to ensure the decoupling between the

transmitting coil and compensation coils, therefore reducing the impact of redundant coupling on the system's transmission efficiency.

2) The differences in magnetic field intensity between the integrated and traditional structures were analyzed via finite element simulation under aligned and offset scenarios. The results showed that the integrated structure improved the system's transmission efficiency in both cases. A simulated human body model was established to evaluate the system's safety. Simulation results showed that the peak electric field strength in human tissue was 0.078 V/m, and the peak magnetic field intensity was 3.07 A/m, both of which comply with human safety standards.

3) A series multi-coil magnetically integrated experimental WPT system for cardiac pacemakers was constructed. Experimental results showed that the maximum transmission efficiency could reach 57.87%, with an output power of 1.14 W under horizontal misalignment whereas the traditional non-integrated structure achieved a maximum efficiency of only 44.09%, with an output power of only 0.82 W. A 13% maximum transmission efficiency improvement was achieved by the proposed integrated system under offset conditions. Compared to the system employing traditional non-integrated LCC-S compensation topology, the integrated structure maintained a approximately same transmission efficiency and effectively reduced the volume of the secondary side circuit, making it suitable for biomedical implantation applications.

ACKNOWLEDGEMENT

2023 Liaoning Provincial Department of Education Basic Research Project (General Project), Grant/Award Numbers: JYTMS20230815.

REFERENCES

[1] Wang, J., E. G. Lim, M. P. Leach, Z. Wang, R. Pei, Z. Jiang, and Y. Huang, "A 403 MHz wireless power transfer system with tuned split-ring loops for implantable medical devices," *IEEE Transactions on Antennas and Propagation*, Vol. 70, No. 2, 1355–1366, Feb. 2022.

[2] Cao, X., H. Sato, K.-D. Xu, W. Jiang, S. Gong, and Q. Chen, "A systematic method for efficient wireless powering to implantable biomedical devices," *IEEE Transactions on Antennas and Propagation*, Vol. 71, No. 3, 2745–2757, Mar. 2023.

[3] Han, W., K. T. Chau, C. Jiang, and W. Liu, "Accurate position detection in wireless power transfer using magnetoresistive sensors for implant applications," *IEEE Transactions on Magnetics*, Vol. 54, No. 11, 1–5, Nov. 2018.

[4] Cetin, S. and Y. E. Demirci, "High-efficiency LC-S compensated wireless power transfer charging converter for implantable pacemakers," *International Journal of Circuit Theory and Applications*, Vol. 50, No. 1, 122–134, Jan. 2022.

[5] Khan, S. R., S. R. Khan, G. Cummins, and M. P. Y. Desmulliez, "Wireless power transfer techniques for implantable medical devices: A review," *Sensors*, Vol. 20, No. 12, 3487, Jun. 2020.

[6] Nithiyanandam, V. and V. Sampath, "Approach-based analysis on wireless power transmission for bio-implantable devices," *Applied Sciences*, Vol. 13, No. 1, 415, Jan. 2023.

[7] Yi, P., L. Zhu, L. Zhu, Z. Xiao, Z. Han, and X.-G. Xia, "Joint 3-D positioning and power allocation for UAV relay aided by geographic information," *IEEE Transactions on Wireless Communications*, Vol. 21, No. 10, 8148–8162, Oct. 2022.

[8] Campi, T., S. Cruciani, F. Maradei, A. Montalto, F. Musumeci, and M. Feliziani, "EMI in a cardiac implantable electronic device (CIED) by the wireless powering of a left ventricular assist device (LVAD)," *IEEE Transactions on Electromagnetic Compatibility*, Vol. 63, No. 4, 988–995, Aug. 2021.

[9] Zhang, J., R. Das, J. Zhao, N. Mirzai, J. Mercer, and H. Heidari, "Battery-free and wireless technologies for cardiovascular implantable medical devices," *Advanced Materials Technologies*, Vol. 7, No. 6, 2101086, Jun. 2022.

[10] Zhao, J., Y. H. Zhao, Z. J. Wu, *et al.*, "Electromagnetic compatibility and thermal effects of electric vehicle wireless charging system on cardiac pacemakers," *Transactions of China Electrotechnical Society*, Vol. 37, No. S1, 1–10, Jun. 2022.

[11] Xiao, C., D. Cheng, and K. Wei, "An LCC-C compensated wireless charging system for implantable cardiac pacemakers: Theory, experiment, and safety evaluation," *IEEE Transactions on Power Electronics*, Vol. 33, No. 6, 4894–4905, Jun. 2018.

[12] Li, Y., S. Shi, X. Liu, *et al.*, "Overview of magnetic coupling mechanism for wireless power transfer," *Transactions of China Electrotechnical Society*, Vol. 36, No. S2, 389–403, Dec. 2021.

[13] Zhang, Y., L. Wang, Y. Guo, and C. Tao, "Null-coupled magnetic integration for EV wireless power transfer system," *IEEE Transactions on Transportation Electrification*, Vol. 5, No. 4, 968–976, Dec. 2019.

[14] Gu, Y., J. Wang, Z. Liang, and Z. Zhang, "Communication-free power control algorithm for drone wireless in-flight charging under dual-disturbance of mutual inductance and load," *IEEE Transactions on Industrial Informatics*, Vol. 20, No. 3, 3703–3714, Mar. 2024.

[15] Zhang, Y., T. Kan, Z. Yan, Y. Mao, Z. Wu, and C. C. Mi, "Modeling and analysis of series-none compensation for wireless power transfer systems with a strong coupling," *IEEE Transactions on Power Electronics*, Vol. 34, No. 2, 1209–1215, Feb. 2019.

[16] Yuan, Z., M. Saeedifard, C. Cai, Q. Yang, P. Zhang, and H. Lin, "A misalignment tolerant design for a dual-coupled LCC-S-compensated WPT system with load-independent CC output," *IEEE Transactions on Power Electronics*, Vol. 37, No. 6, 7480–7492, Jun. 2022.

[17] Xiao, C., S. Hao, D. Cheng, and C. Liao, "Safety enhancement by optimizing frequency of implantable cardiac pacemaker wireless charging system," *IEEE Transactions on Biomedical Circuits and Systems*, Vol. 16, No. 3, 372–383, Jun. 2022.

[18] Mahmood, A. I., S. K. Gharghan, M. A. A. Eldosoky, M. F. Mahmood, and A. M. Soliman, "Wireless power transfer based on spider web-coil for biomedical implants," *IEEE Access*, Vol. 9, 167 674–167 686, Dec. 2021.

[19] Mukherjee, D. and D. Mallick, "Magnetoelectric wireless power transfer system for biomedical implants," in *2021 IEEE International Midwest Symposium on Circuits and Systems (MWSCAS)*, 356–359, Sep. 2021.

[20] Kan, T., T.-D. Nguyen, J. C. White, R. K. Malhan, and C. C. Mi, "A new integration method for an electric vehicle wireless charging system using LCC compensation topology: Analysis and design," *IEEE Transactions on Power Electronics*, Vol. 32, No. 2, 1638–1650, Feb. 2017.

[21] Luo, Z. and X. Wei, "Analysis of square and circular planar spiral coils in wireless power transfer system for electric vehicles," *IEEE Transactions on Industrial Electronics*, Vol. 65, No. 1, 331–341, Jan. 2018.

[22] International Commission on Non-Ionizing Radiation Protection (ICNIRP), , "ICNIRP Statement-Guidelines for limiting ex-

posure to time-varying electric, magnetic, and electromagnetic fields (1 kHz to 100 kHz)," *Health Physics*, Vol. 74, No. 4, 818–836, 2010.

[23] Seo, S., H. Jo, and F. Bien, "Free arrangement wireless power transfer system with a ferrite transmission medium and geometry-based performance improvement," *IEEE Transactions on Power Electronics*, Vol. 35, No. 5, 4518–4532, May 2020.

[24] "IT'IS Foundation — Database at a Glance." [Online]. Available: https://itis.swiss/virtual-population/tissue-properties/database/dielectric-properties/

[25] Kod, M., J. Zhou, Y. Huang, M. Stanley, M. N. Hussein, A. P. Sohrab, R. Alrawashdeh, and G. Wang, "Feasibility study of using the housing cases of implantable devices as antennas," *IEEE Access*, Vol. 4, 6939–6949, Sep. 2016.

[26] Cetin, S. and Y. E. Demirci, "High-efficiency LC-S compensated wireless power transfer charging converter for implantable pacemakers," *International Journal of Circuit Theory and Applications*, Vol. 50, No. 1, 122–134, Jan. 2022.